Accepted Manuscript

Determination of two-dimensional space-time correlations in jet flows using simultaneous PIV and LDV measurements

F. Kerhervé, J. Fitzpatrick, J. Kennedy

PII: S0894-1777(10)00010-5
DOI: 10.1016/j.expthermflusci.2010.01.008
Reference: ETF 7296

To appear in: *Experimental Thermal and Fluid Science*

Received Date: 8 June 2009
Revised Date: 16 December 2009
Accepted Date: 19 January 2010

Please cite this article as: F. Kerhervé, J. Fitzpatrick, J. Kennedy, Determination of two-dimensional space-time correlations in jet flows using simultaneous PIV and LDV measurements, *Experimental Thermal and Fluid Science* (2010), doi: 10.1016/j.expthermflusci.2010.01.008

Determination of two-dimensional space-time correlations in jet flows using simultaneous PIV and LDV measurements

F. Kerhervé[*,a], J. Fitzpatrick[**,b], J. Kennedy[c,1]

[a]Laboratoire d'Etudes Aérodynamiques, Université de Poities - ENSMA 6609 CNRS, 43 rue de l'Aérodrome, 86036 Poitiers Cedex, France
[b]School of Engineering, Trinity College Dublin, Ireland
[c]School of Engineering, Trinity College Dublin, Ireland

Abstract

The two-dimensional space-time turbulence statistics of free shear jet flows in the form of the two-point velocity correlation tensor are important for aeroacoustic noise source modelling based on the acoustic analogy approach. This paper presents a direct application of the Point Referenced Global Correlation (PRGC) technique to measure the components of this correlation tensor for a sector of the flow field in two jet configurations. The PRGC approach combines single point and global measurement techniques and enables two-point space-time correlations over a region of the flow to be obtained. The technique is applied to a single stream jet and a co-axial coplanar jet at a Mach number of 0.24 using commercial Laser Doppler velocimetry (LDV) and low-speed Particle Image velocimetry (PIV) systems. Results for the 1-D correlations are shown to compare well with two point measurements. The results for the 2-D space time correlations

[*]Dr.,franck.kerherve@lea.univ-poitiers.fr, +33(0)549366086, Corresponding author
[**]Prof., john.fitzpatrick@tcd.ie
[1]PhD., john.kennedy@tcd.ie

are presented and the characteristics for both configurations discussed.

1. Introduction

The two-point space time correlations of turbulent jets are a key element in acoustic analogy approaches for noise source modelling based on the work of Lighthill (1952). In Lighthill's theory, the dynamics of the far field noise of a jet can be related to its intrinsic turbulence through the use of the fourth-order velocity correlation tensor. This tensor can be considered to represent the dynamics and the efficiency of the mechanisms of conversion of the turbulence kinetic energy into acoustic energy. Thus, a key element in the acoustic analogy is the correlation tensor (Goldstein 1976) and this needs to be determined and modelled as accurately as possible to account for the intrinsic physics of the source terms. In general, the two-point statistical properties have been determined using second order correlations from two-point measurements as proposed by Ribner (1969). The results for these have been reported using hot-wire anemometry (HWA) by Davies et al. (1963) and Chu (1966), Laser Doppler Velocimetry (LDV) by Lau (1980) and Kerhervé et al (2004), optical field measurement techniques such as particle image velocimetry (PIV) as used by Hu et al. (2002), Bridges & Wernet (2002) and Fleury et al. (2007) or optical deflectometry as reported by Doty & McLaughlin (2005). The first two use single point measurements so that a large number of measurements are necessary to provide sufficient information on the flow field statistics. The last two provide a global measurement of the flow field so that the required statistical information can be more readily acquired although the data post processing can be extensive. However the second group still remains limited in terms of temporal resolution especially in high speed flow cases.

The determination of auto and cross spectra and the frequency dependence of the length scales and convection velocities required for more effective noise predictions as has been reported by Morris & Boluriaan (2004), Self (2004) and Bassetti & Morfey (2007) can only realistically be determined at present using LDV or HWA measurements especially at higher frequencies. Although global measurement techniques (PIV) are efficient when the flow needs to be examined over a large area, the relatively low repetition rate means that temporal-related turbulence properties can only be obtained using restrictive assumptions based on the Taylor frozen-flow approximation (e.g. Batchelor 1953) applicable for well defined coherent structures only. In the near future, with the ongoing development of high speed cameras, the determination of the frequency dependent properties from global measurement techniques will be achievable. The use of dual-PIV recently reported by Fleury et al (2007) and applied to a free jet flow can offer an alternative to high-speed camera systems. The use of these global techniques to determine the more subtle aspects of the turbulent statistics requires substantial data processing and it is still considered more efficient to employ them in combination with single point measurements.

The Point-Referenced Global Correlation (PRGC) technique proposed by Chatellier & Fitzpatrick (2005) has been shown to be an efficient method for determining the global space-time correlations for turbulent flows using PIV with single point measurements. It provides an extremely efficient method for establishing the space-time correlations of turbulence in flows compared with the normal two single point procedures which require significantly more measurements. The statistical errors associated with the application of the PRGC have been detailed by Kerherve et al (2008) and in the present paper, the method is used to determine the space-time correlations over a large area of the flow using PIV and LDV measurements obtained in single stream and co-axial round jets at a Mach number of 0.24. The two-dimensional space-time correlation representative of both longitudinal and radial turbulence velocity fluctuations are determined and the temporal dynamics of the 2D-spatial decay are discussed. The effect of nozzle configuration on the flow features such as the turbulence integral length and time scales and the anisotropy of the energy containing turbulence are presented and discussed.

2. Two dimensional space-time correlations

Two point 2D space-time correlation functions often referred to as the spatio-temporal correlations are given by

$$R_{ij}(\vec{x},\vec{s},\tau) = \int_{-\infty}^{+\infty} u_i(x,t)u_j(\vec{x}+\vec{s},t+\tau)dt \tag{1}$$

where u_i is the i-th component of the instantaneous turbulent velocity, $\vec{x}$ the reference point location, $\vec{s}$ the spatial separation vector and τ the time delay between the two point measurements The normalised correlation or cross co-variance function is more commonly used and this is given by

$$r_{ij}(\vec{x},\vec{s},\tau) = \frac{R_{ij}(\vec{s},\tau)}{\left[R_{ij}(0,0,0)R_{ij}(0,\vec{s},0)\right]^{1/2}} \tag{2}$$

where the denominator is the square root of the product of the variance of the two measurements. It is from these that the spatial and temporal properties of the turbulence can be determined as detailed by, for example, Townsend (1974) or Tennekes & Lumley (1972). In the first instance, the correlation length scales in a fixed reference frame can be determined as a function of separation from

$$\ell_{ij}(\vec{x},\vec{s}) = r_{ij}(\vec{x},\vec{s},0) = \frac{R_{ij}(\vec{x},\vec{s},0)}{\left[R_{ii}(\vec{x},0,0)R_{jj}(\vec{x},s,0)\right]^{1/2}} \tag{3}$$

and, from this, the integral length scale at point location $\vec{x}$ in the j-th direction and relative to the i-th velocity component is obtained as

$$\lambda_{ij}(\vec{x}) = \int_0^{+\infty} \ell_{ii}(\vec{x}, s_j) ds_j \tag{4}$$

The time scales for the turbulence are determined by plotting the peak value for each of the family of correlations as a function of the associated time lag giving a function $\hat{r}_{ij}(\vec{x}, \vec{s}, \hat{\tau})$, where $\hat{r}_{ij}$ is the maximum for each value of $\vec{s}$ occuring at time lag $\hat{\tau}$. The integral time scale relative to the i-th velocity component and in the j-th direction is then given by,

$$\tau_{ij}(\vec{x}) = \int_0^{+\infty} \hat{r}_{ii}(\vec{x}, s_j, \hat{\tau}) d\hat{\tau} \tag{5}$$

The time delay $\hat{\tau}$ associated with the maximum of each normalised correlation function gives the mean or bulk convection velocity U_c -in the case of flow jets this quantity reduces to its axial component-, from

$$U_c = |s_1|/\hat{\tau} \tag{6}$$

It should also be noted that the length scale in a moving reference frame (i.e. Lagrangian) is given by

$$\lambda^*_{ij}(\vec{x}) = \int_0^{+\infty} \hat{r}_{ii}(\vec{x}, s_j, \hat{\tau}) ds_j \tag{7}$$

The time scale and the moving reference length scale are directly related via the convection velocity.

3. Experimental Set Up, Instrumentation and Signal Analysis

3.1. Experimental rig

The experiments were performed in the subsonic open jet facility at Trinity College Dublin as described by Chatellier & Fitzpatrick (2005). A 50 mm diame-

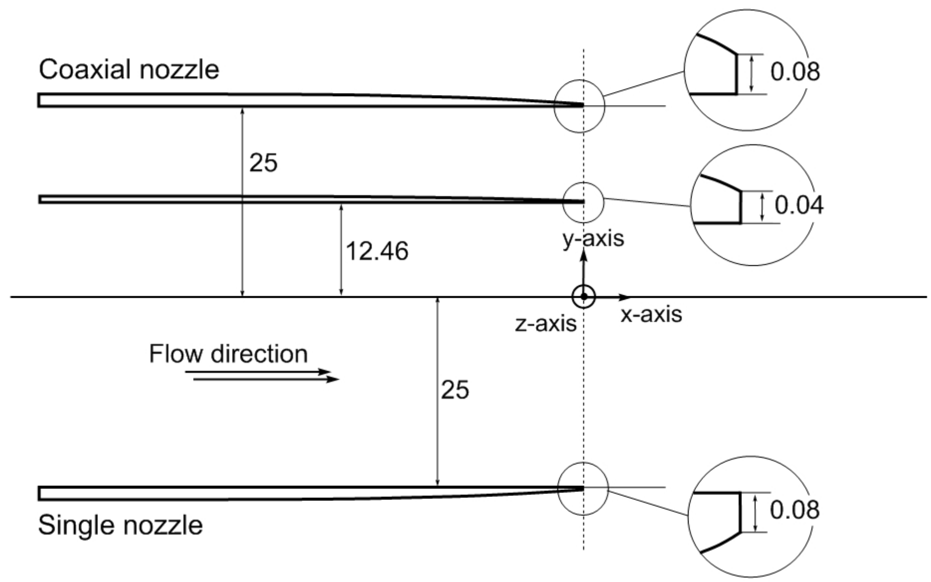

Figure 1: Detail of the nozzle configurations (dimensions in mm): (top half) coaxial nozzle, (bottom half) single nozzle.

ter jet discharges into quiescent air from a plenum through an elliptical bell-mouth with jet exit velocities from 30 m/s to 80 m/s and associated Reynolds numbers based on the exit nozzle diameter between 10^5 and 3×10^5. An arrangement of honeycombs and screens followed by the bell-mouth ensures that the flow in the nozzle has a low turbulence level and is aerodynamically uncoupled with the upstream fan. Two 160mm-long nozzle configurations were installed in the rig for the current tests, a single jet and a co-axial coplanar nozzle the geometric details of which are shown in figure 1 with the flow exit conditions given in Table 1. Both jets were at ambient temperature with an exit velocity of 80 m/s for the primary flow.

Nozzle Type	D_p (mm)	D_s (mm)	U_p (m/s)	U_s (m/s)	T_p/T_o	T_s/T_o	Re_p	Re_s
Single	-	50	-	80	-	1	-	$2.6.10^5$
Coxaial	25	50	80	50	1	1	$1.3.10^5$	$8.3.10^4$

Table 1: Flow conditions for the single and coplanar round nozzles: (D_p,D_s) primary and secondary nozzle diameters, (U_p,U_s) primary and secondary jet nozzle velocity exit, (T_p/T_o,T_s/T_o) primary and secondary nozzle temperature ratios, (Re_p,Re_s) primary and secondary nozzle exit Reynolds numbers.

3.2. Optical set-up

The measurements were obtained using commercial PIV and LDV systems as described below and a schematic of the set-up for the experiments is shown in figure 2.

The LDV system consists of a 500mW Argon-ion Laser and a dual beam Dantec optical head with blue (488mm) and green (514nm) wavelengths for radial and longitudinal velocity components respectively. Dimensions of the measurement volumes for both wavelengths are (0.12×0.12×1.6) mm^3 - the largest dimension corresponding to the measurement volume length. To optimise data sample rates and signal-to-noise ratios, the system was operated in the forward scatter mode. The receiving lens was located in front of the beam head at an off-axis angle of some 30°. A pinhole of approximately 0.1mm diameter in the receiving optic is used to collect the scattered light and to reduce the third dimension of the measurement volume. Data collected are analysed using a Dantec burst spectrum analyser type BSA F50 to provide instantaneous velocity information.

The PIV system combines a double-pulsed Nd:Yag Laser (New-Wave Solo II, 15mJ, 15Hz, 532nm), a double-exposure camera (LaVision Flowmaster 3, 12bit, 1280×1024 $pixel^2$) and the LaVision DaVis software. The camera is located in

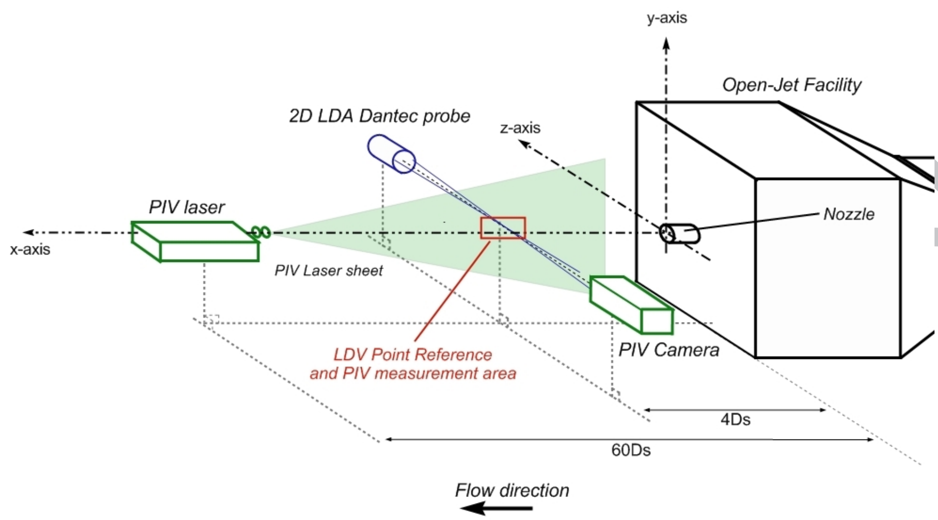

Figure 2: General schematic of the experimental set-up.

front of the LDV optical head as shown in figure 2. To reduce reflections and glare on the PIV images due to the LDV beams, two narrow-band filters (532nm and 10nm width) are used on the camera and the power of the LDV laser beams is slightly reduced. The intensity of light reaching the CCD camera is consequently reduced but the high sensitivity of the CCD sensor and reduction of the beam intensity levels enables good quality images to be recorded as detailed by Chatellier & Fitzpatrick (2005). The flow area investigated by the PIV was 2Ds$\times$0.8Ds (where Ds is the outer nozzle diameter) corresponding to 1152$\times$480 pixels^2. PIV images were computed using classical window shifting and multigrid techniques (64$\times$64 down to 16$\times$16 pixels^2 with 50% overlap). The final vector images contain 144$\times$60 vectors at a resolution of 0.68mm. A systematic detection process of spurious PIV vectors based on the adapted median test proposed by Westerweel & Scarano (2000) is applied on each PIV instantaneous velocity field. The average number of rejected vectors represents less than 5% of the total vectors.

The LDV beams are focused at the centre of the PIV measurement region and this is the point-reference around which the 2D space-time correlations are calculated. For each location examined, 6 sets of 250 PIV images are recorded at 8Hz simultaneously with a 45s long LDA signal. The PIV and LDV systems are triggered together such that the PIV shot times are recorded on an additional channel for the BSA processor. For each of these sets, 2D space-time correlations between the LDV point-reference and the different points of the PIV images are calculated and averaged over the six sets in order to reduce noise in the data. The mean sampling frequencies for the LDA signals for the different locations of the flow examined vary between 25kHz and 70kHz for the longitudinal velocity component (green wavelength) and between 8kHz and 17kHz for the radial velocity component (blue wavelength). As shown by Kerhervé et al (2008), more noise may be thus expected in the correlation estimate associated with the radial component. For the PRGC procedure, a lower LDV mean sampling frequency causes a reduction of the number of LDV samples. Since this procedure uses the slotting technique of Muller et al (1998), as we'll discussed shortly, the number of samples is effictively an important parameter on which the quality of the estimate directly depends.

For the flow seeding, an Antari Z300 fog generator which generates particles of approximately $1\mu m$ diameter has been used. To reduce bias error due to inhomogeneous seeding over all of the region examined, both the main flow and the surrounding medium were seeded simultaneously.

One challenging aspect in the measurement set up is the alignment of both optical systems. For the correlation at zero time delay and zero separation to be unity as required, the assumption is that the location of the LDV measurement would correspond exactly to a point of the PIV grid. In practice, this is difficult to achieve. The correlation with zero separation distance must therefore be considered as missing and the noise-floor undetermined. However since the absolute locations of the point reference and that of the PIV grid are known, this does not constitue a limitation of the technique. The information lost in terms of correlation length scales due to the lack of zero separation is a function of both the local Taylor micro-scale and the dimension of the PIV interrogation area. The smallest separation between the point reference and that of the PIV grid is between 0mm and 0.34mm -half the vector resolution- which is therefore significantly small for the present purpose.

To optimise the alignment of the LDV location in the PIV measurement plane, the following procedure is systematically employed: (1) the LDV measurement volume is first positioned. This is effected using an optical target centred in the jet exit. Few holes of 0.5mm diameter are inserted into the target at the exact location where point reference measurement are required, (2) the alignment of the PIV laser sheet with both the jet exit and the LDV measurement volume is then effected using a piece of thread of approximately 0.2mm diameter centred on the jet nozzle -at this stage, the PIV laser is aligned with the jet nozzle and contains the point measurement-, (3) the focus of the PIV camera is then adjusted using the optical target again with the LDV measurement volume easily identified as a black spot in the PIV image.

The correlations at zero time delay and assumed zero spatial separation were found to vary between 0.7 and 0.9 for the longitudinal turbulence velocity component although greater discrepancies were observed for the radial component of the velocity where correlations of 0.5 to 0.75 were obtained depending on the location in the flow. This is not unusual as the decay of the correlation function in the cross flow direction would be expected to be somewhat greater than that in the streamwise direction (Davies et al 1963).

3.3. Point-Referenced Global Correlation technique

The Point-Referenced Global Correlation (PRGC) technique developed by Chatellier & Fitzpatrick (2005) enables the space-time velocity correlations in a 2D region to be obtained using PIV output with point measurement data. The technique enables the correlation of the randomly sampled LDV data with the undersampled velocity data at each point in the PIV field using the slotting technique described by Muller et al (1998). The correlation estimate between the LDV point reference, say $\vec{x}$ of fluctuating velocity component $u_{LDV,i}$, and a point of the PIV grid, say $\vec{x}+\vec{s}$, of fluctuating velocity component $v_{PIV,j}$ is given by,

$$
\begin{aligned}
r_{ij}(\vec{x},\vec{s},\tau_k) = & \left[\sum_{m=1}^{M_{LDV}}\sum_{n=1}^{N_{PIV}} u_{LDV,i}(\vec{x},t_{u,m}) v_{PIV,j}(\vec{x}+\vec{s},t_{v,m}) w_k(t_{v,n}-t_{u,m})\right] \\
& \times \left[\sum_{m=1}^{M_{LDV}}\sum_{n=1}^{N_{PIV}} u_{LDV,i}(\vec{x},t_{u,m})^2 w_k(t_{v,n}-t_{u,m})\right]^{-1} \\
& \times \left[\sum_{m=1}^{M_{LDV}}\sum_{n=1}^{N_{PIV}} u_{PIV,j}(\vec{x},t_{v,m})^2 w_k(t_{v,n}-t_{u,m})\right]^{-1}
\end{aligned}
$$

where τ_k is the k-th retard time step equal to $k\Delta\tau$, $\Delta\tau$ being the temporal resolution of the estimate, M_{LDV} and N_{PIV} denote the number of LDV samples and PIV images respectively, $t_{v,n}$ and $t_{u,m}$ represent n-th and m-th time steps of the LDV and PIV signals respectively. The weighting window w_k given by,

$$
w_k(t_{v,n}-t_{u,m}) = \begin{cases} 1-|(t_{v,n}-t_{u,m})/\Delta\tau - k| & \text{if } |(t_{v,n}-t_{u,m})/\Delta\tau - k| < 1 \\ 0 & \text{otherwise} \end{cases}
$$

is necessary to reduce the slot quantisation noise and consequently the variance of the estimate (Nobach et al 1998). The space-time evolution of the velocity correlation is reconstructed over the PIV region and the technique has been benchmarked by Chatellier & Fitzpatrick (2005) and Kerhervé et al (2008) using both simulated and experimental data. It was shown that a PIV repetition rate of few Hertz can be correlated with LDV data to provide spatio-temporal correlation information at the spatial resolution of the PIV and the temporal resolution of the LDV. Additionnaly, it was reported by Chatellier & Fitzpatrick (2005) that a potential source of error may be high velocity gradients in the shear layer which are not resolved by the PIV system. Particular attention has been paid in the present paper to ensure that both the PIV and LDV measurements exhibit similar characteristics in respect of measured mean velocity gradients. Finally, as discussed by Chatellier & Fitzpatrick who examined the error estimate of the PRGC technique for the present flow examined, the theroretical absolute error of the correlation estimate reaches a value of 1.25×10^{-3} (figure 7 of the cited paper), which is sufficiently small to obtain accurate results. The theoretical error was formalised on the basis of cross-correlation function taking the form of an exponential-cosine, which for turbulent flows offers a good description of the two-point temporal statistics.

4. Results

4.1. Preliminary measurements

A series of measurements were made using the LDV system to characterise the mean flow properties of both jets. The mean and rms longitudinal velocity profiles (normalised by the nozzle exit velocity, using the primary flow for the coaxial jet) are shown in figures 3 and 4 respectively for both jets. For the single jet, the potential core extends to around $5.5D_s$ -where D_s is the secondary exit nozzle diameter- downstream with the shear layer expanding with an angle of about 5°. Along the nozzle lip line, turbulence levels of 16% of the jet exit velocity are observed beyond $2D_s$ consistent with the findings of, for example, Jung (2004) and Hussain (1981) while turbulence in the centre of the potential core is less than 1%. The initial mixing region immediately downstream from the exit nozzle extends up to about $1.5D_s$. This is longer than expected but may result from the low Reynolds number of the flow and may explain the long potential core observed and the low expanding degrees of the shear layer compared to the results of Lau et al. (1979).

For the co-axial jet, the primary potential core was found to be significantly shorter than that for the single stream jet since as it extended to $4.5Ds$ which is a few diameters beyond the region where the primary and secondary shear layers merged so that the jet begins to behave as a single stream jet. This compares well with the findings of Ko & Kwan (1976). It can be seen from figure 4 that both shear layers expand with a linear rate of growth as has been reported by again Ko & Kwan (1976). The asymmetry observed in the RMS maps may be related to the presence of the winglets in the upstream region of the nozzle exit positioned at 120° from each other between the primary and secondary nozzles. Reduction in the peak level of turbulence when compared to the single stream jet can be observed in figure 4(b) where a maximum of 12% of the primary jet exit velocity is observed indicating efficient mixing and dissipation.

The axial evolution of the momentum and vorticity thicknesses were determined

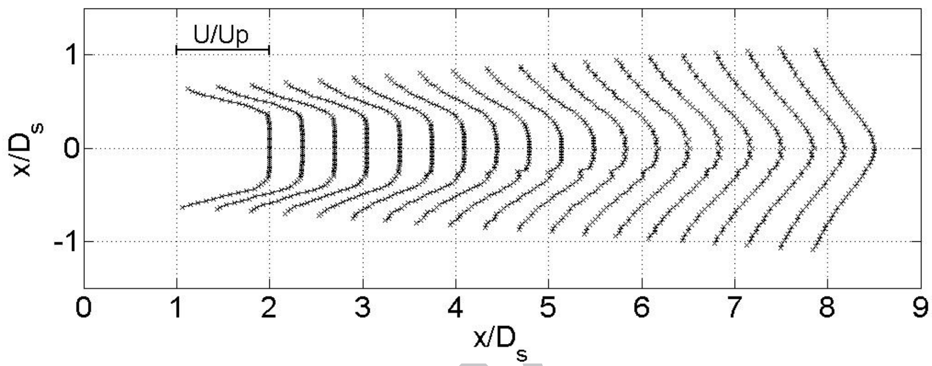

(a) Single stream jet

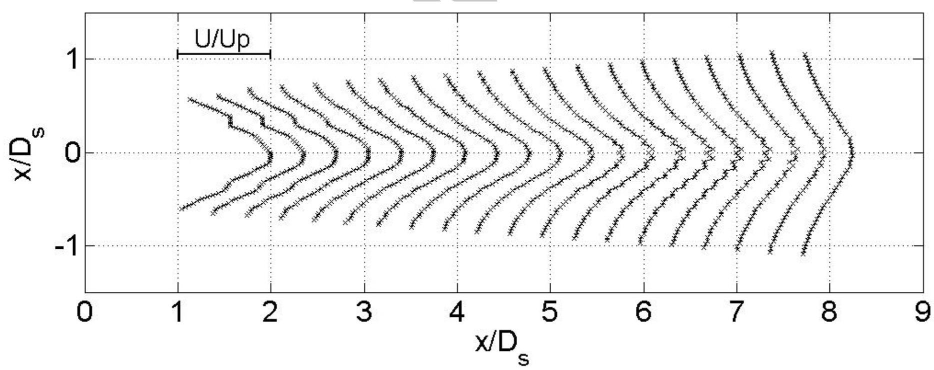

(b) Coplanar jet

Figure 3: Mean longitudinal velocity profiles for *(a)* the single stream jet and *(b)* the coplanar jet.

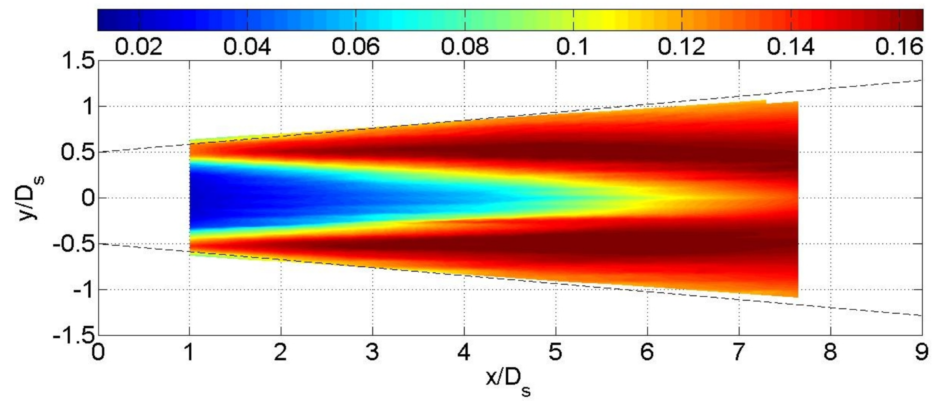

(a) Single stream jet

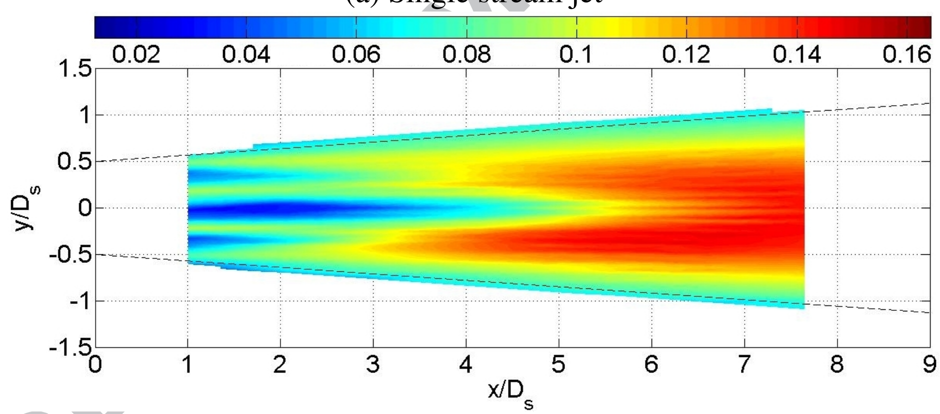

(b) Coplanar jet

Figure 4: RMS longitudinal velocity profiles normalised by secondary jet exit velocity for *(a)* the single stream jet and *(b)* the coplanar jet.

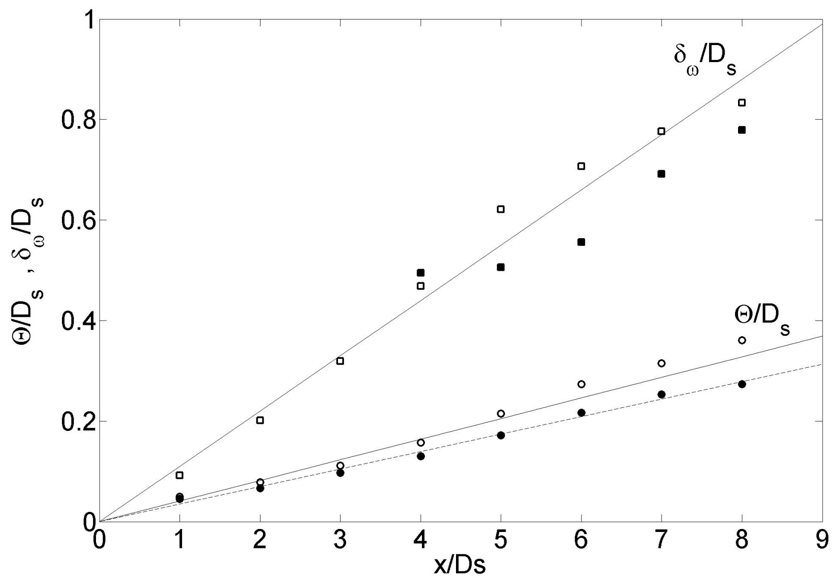

Figure 5: Momentum and vorticity thicknesses as a function of distance from nozzle exit for (open symbols) the single stream jet and (filled symbols) the coplanar jet.

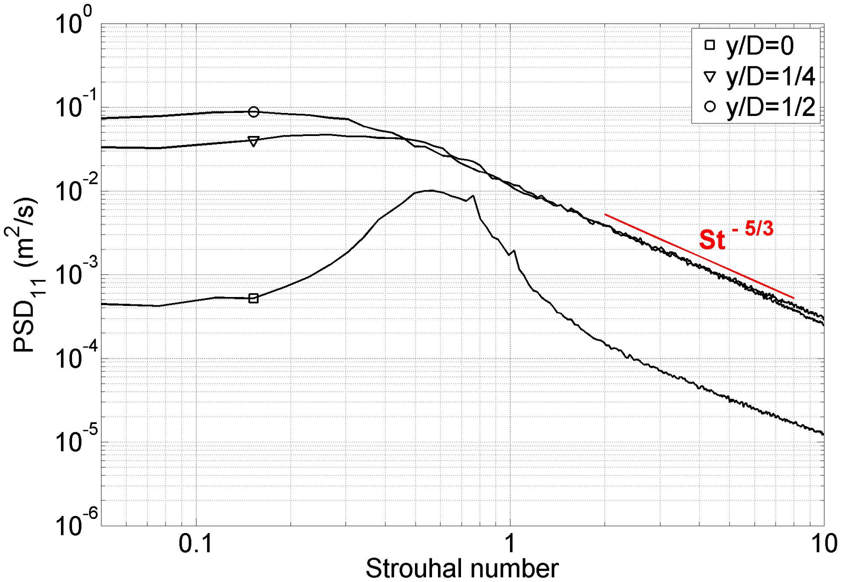

(a) Single stream

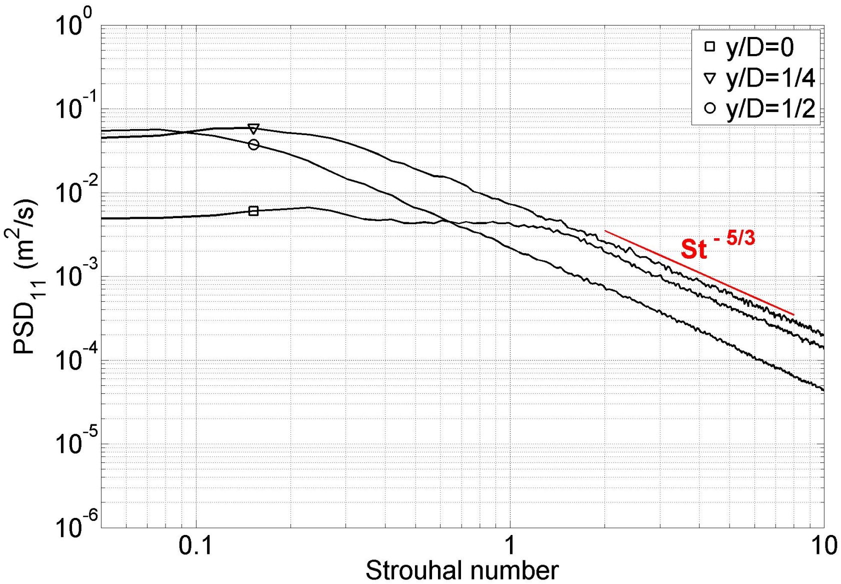

(b) Coplanar jet

Figure 6: Turbulence spectra at 4Ds downstream in *(a)* single stream jet and *(b)* coplanar jet.

using the common definitions,

$$\Delta\theta = \int_0^\infty \frac{U(y)}{U_s}\Big(1 - \frac{U(y)}{Us}\Big)dy \tag{8}$$

$$\delta_\omega = U_s / \Big(\frac{\partial U(y)}{\partial y}\Big)_{max} \tag{9}$$

where $U(y)$ denotes the local mean velocity and U_s the secondary exit velocity. The results for these are reported in figure 5. For the single jet, both quantities increase linearly with the distance from the nozzle exit representating of the growth of the shear layer and most energetic flow structures. The values for $d\theta/dx$ and $d\omega/dx$ of 0.041 and 0.11 respectively compare well with the results reported by Laurendeau (2007), Liepmann & Laufer (1947) and Ricaud (2003). The values for the co-axial jet were determined for the overall shear layer including both primary and secondary elements and are very similar to the single jet case.

The auto-spectra of the longitudinal velocity for the single jet are reported in figure 6(a) at $4Ds$ downstream from the jet exit for three radial positions (y/Ds = 0, 0.25, 0.5) and these show characteristics typical of the potential core and shear layer regions of the flow as described by example by Jordan & Gervais (2005) and Lau (1980). The jet instability towards the end of the potential core is clear from the centre-line measurement and the associated Strouhal number of 0.53 agrees well with that reported by Delville et al. (1999). The auto-spectra for the longitudinal velocity in the co-axial jet shown in figure 6(b) show no evidence of the jet instability. There is an increase in the turbulence intensity along the centreline at the higher frequencies indicating enhanced increased mixing in this region with an accompanying decrease along the outer lip line. The absence of noticeable instability along the coaxial jet centreline at $4D_s$ indicates that the local turbulence is already predominent and that the overall flow is more rapidly desorganised than that of the examined single jet.

4.2. 1-D space-time correlations

A series of measurements were performed in the single stream jet using the PIV/LDV set up and the 1-D space-time correlations were obtained using the PRGC method. Additional two-point measurements combining the LDV system with a cross hot wire probe were made to assess the accuracy of the correlation estimates obtained with the PRGC technique. The hot-wire probe is a Dantec type H32 connected to two DISA 55M01 constant temperature anemometers with a common trigger. The LDV probe is located upstream and maintained fixed while the hot-wire probe moved downstream for a range of separation distances. Special attention has been paid that the seeding do not contaminate the hot wire measurements. Direct comparisons of the space-time correlation obtained via the PRGC technique and the two-point measurements for various axial separation distances are plotted in figure 7. While some discrepancies are found for large time delays, the results indicate a very good agreement showing that the PRGC technique is able to capture statisticaly the space-time decrease of the turbulence accurately. Comparisons between the turbulence velocity cross-correlation at the point-reference -which refers strickly speaking to an auto-correlation function at zero separation- obtained from the LDV signal and the PRGC technique considering zero separation is reported in figure 8(a) for one of the positions considered. While the peak of the PRGC correlation estimate is not unity as expected when correlating two signals recorded by two different anemometers, very good agreement is obtained between both estimates.

The Fourier transforms of these correlations give the turbulence auto-spectrum. A

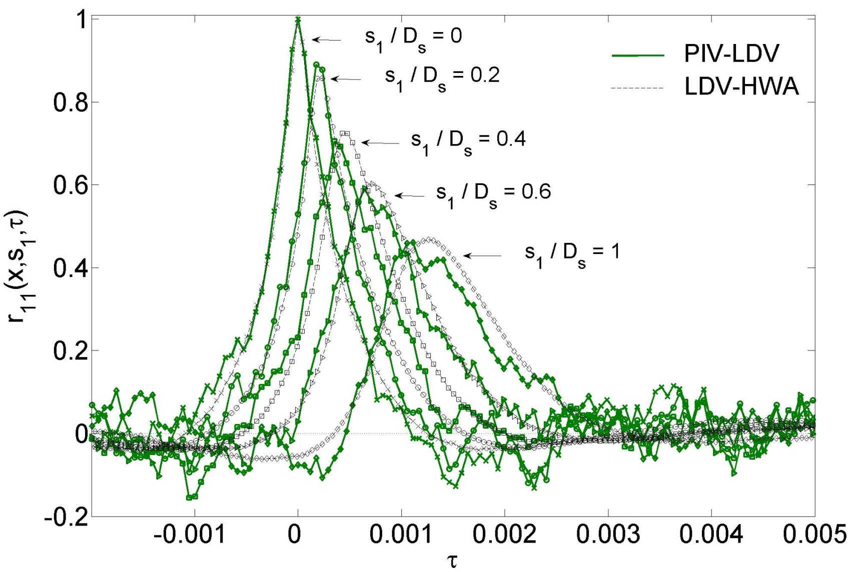

Figure 7: Comparison of space-time correlations (plain line) PRGC, (dashed line) LDV/HWA measurements)

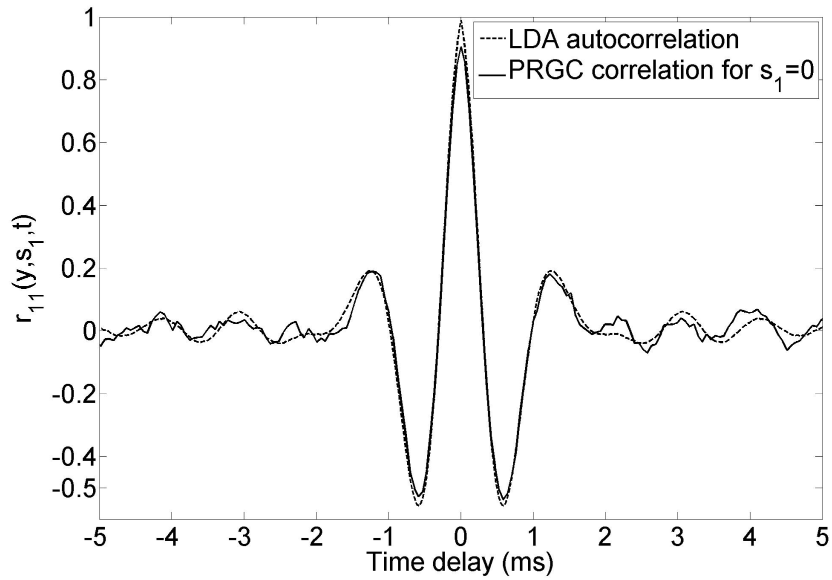

(a) Autocorrelation

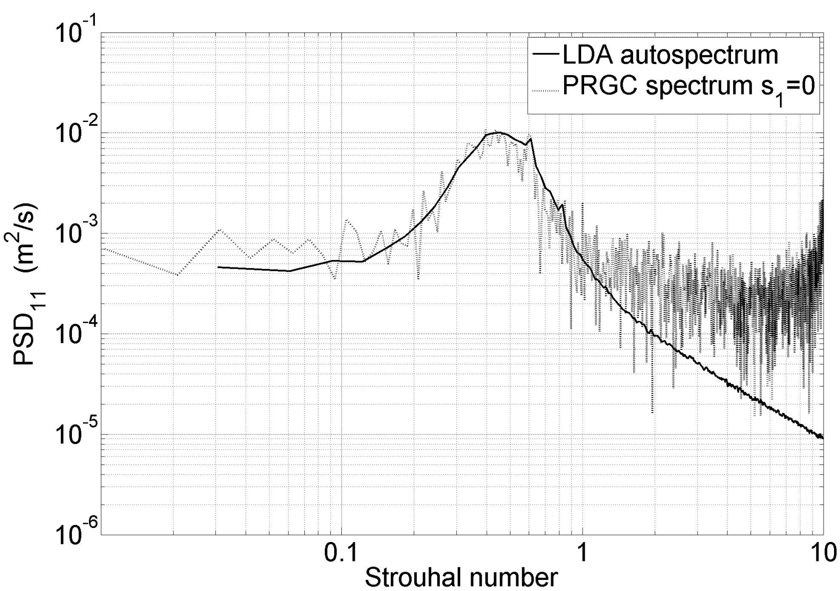

(b) Power spectral density

Figure 8: *(a)* Autocorrelation as a function of time delay and *(b)* auto-spectrum from PRGC and LDV (zero separation) as a function of Strouhal number based on the secondary jet diameter and exit velocity for the single stream jet.

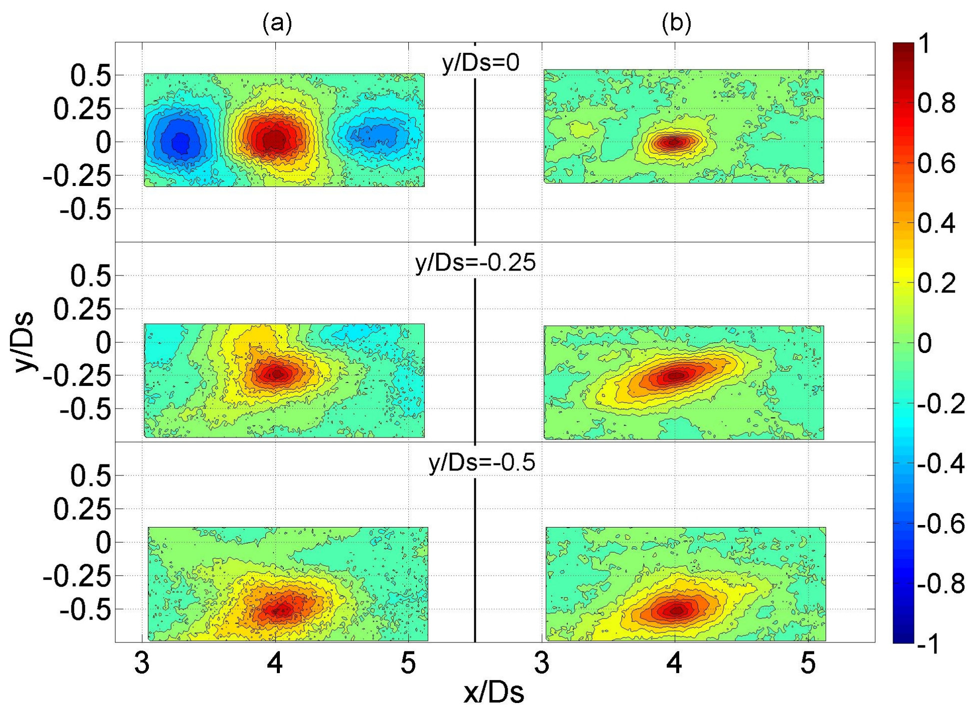

Figure 9: Spatial correlation function for axial velocity component (r_{11}) for the point reference at 3 locations: *(top)* $y/Ds = 0$ jet centreline, *(centre)* $y/Ds = 0.25$, *(bottom)* $y/Ds = 0.5$ nozzle lipline. *(a)* Single stream jet, *(b)* Coaxial jet.

sample of these are reported in figure8(b), showing good agreement for Strouhal number, based on the secondary jet exit velocity and nozzle diameter, below 2.5 -corresponding to 4kHz. The spectra are here given with a Strouhal number -respectively frequency- resolution of 0.03 &0.01 -respectively 48Hz & 16H- for the PRGC technique and the LDV measurement. This is a remarkable result since one may not forget that using the PIV alone would have lead to a spectral estimate valid for frequencies below 3Hz only. Combination of both systems may therefore be seen as an effective way to improve the temporal resolution of the PIV technique.

4.3. 2-D space-time correlations

Although the single stream and coplanar jets exhibit different characteristics at 4*Ds* downstream, this region constitutes an area of active mixing where the shear layers begin to merge in both cases. The region surrounding the end of the potential core is considered by many authors as a dominant region of noise producing events where the collapse of the potential core entrains rapid modifications of the flow field which constitute strong sources of sound (Bogey & Bailly 2005, Hileman et al 2005). As a consequence, two-dimensional correlations were obtained using the PRGC technique at 4*Ds* downstream and three radial locations (y/Ds=0, 0.25 & 0.5) in both jet nozzle configurations and are presented in figures 9 and 10 for the longitudinal and radial turbulent velocity components respectively and in figure 11 for the shear stresses. These correlations are for the velocities at the LDV point reference and the PIV field at zero time delay. For each of the results, the point-reference is located where the maximum of the correlation occurs.

The results in the top row of figures 9(a) & 9(b) show the longitudinal correlations along the jet centerline and these can be seen to be symmetrical about the jet axis. For the single jet case, negative values are observed both upstream and downstream of the correlation maximum. The negative peaks are representative of coherent structures at this location associated with the jet column instability evident in the turbulence spectra of figure 6(a). For the co-axial jet case, these coherent peaks are not evident in figure 6(b) as the turbulence at this location is well developed. The characteristics in figure 9(b) show evidence of axial ”stretching” due to entrainment of the core by the outer jet structure. In the shear layer regions, it can be seen from the centre and lower rows of figure 9(a) for the single jet and figure 9(b) for the co-axial case that the correlations are no longer symmetrical and

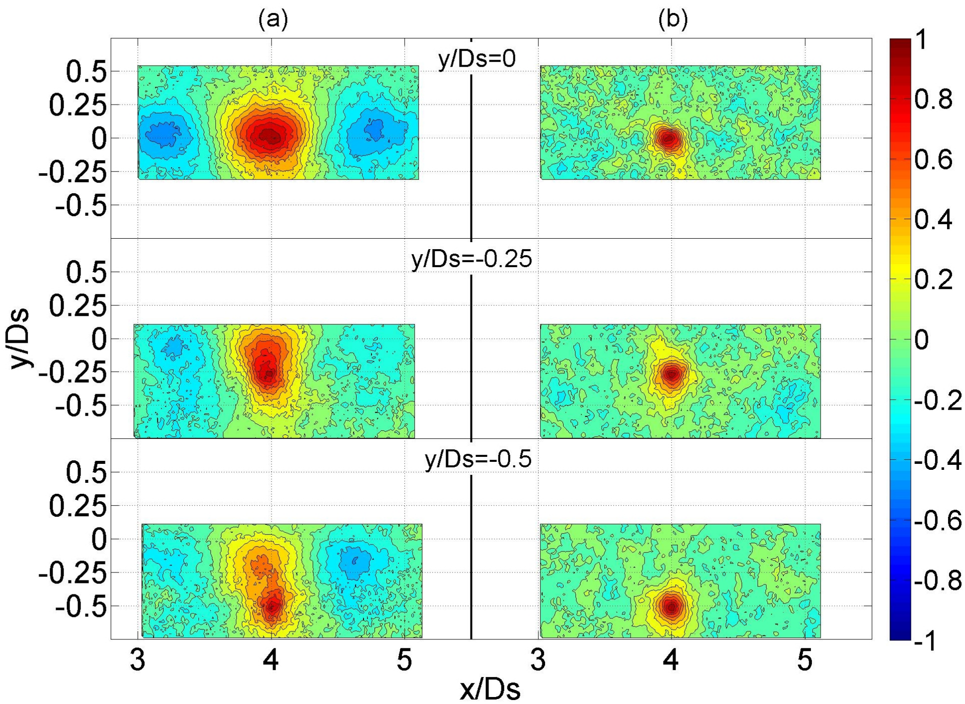

Figure 10: Spatial correlation function for radial velocity component (r_{22}) for the point reference at 3 locations: *(top)* $y/Ds = 0$ jet centreline, *(centre)* $y/Ds = 0.25$, *(bottom)* $y/Ds = 0.5$ nozzle lipline. *(a)* Single stream jet, *(b)* Coaxial jet.

exhibit significant distortion with a realignment of the maxima of the correlation along an axis forming an angle of approximately $\sim 15^\circ$ with the jet centerline. At y/Ds=0.25, the co-axial jet exhibits an elliptic pattern for the space-time correlation whereas the single jet result shows significant distortion. The corresponding PIV images and velocity fields were re-checked to ensure that this was not due to measurement artifacts or spurious vectors but consequence of a physical feature of the flow. This result for a point reference located on the border of the potential core and the shear layer indicates that the turbulence at this location remains correlated with the turbulence on the other side of the potential core. From a mixing

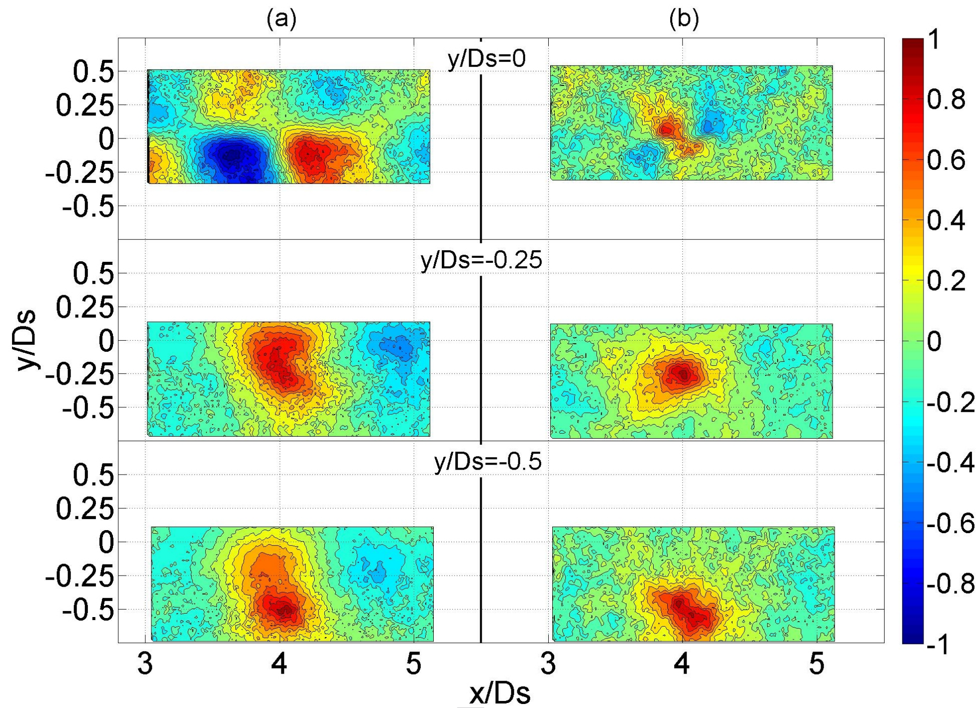

Figure 11: Spatial correlation function for shear stress (r_{12}) for the point reference at 3 locations: *(top)* $y/Ds = 0$ jet centreline, *(centre)* $y/Ds = 0.25$, *(bottom)* $y/Ds = 0.5$ nozzle lipline. *(a)* Single stream jet, *(b)* Coaxial jet.

perspective, this indicates -as expected- the presence of annular coherent scales surrounding the potential core which merge as they develop downstream resulting in the collapse of the potential core.

Along the jet centerline, the radial velocity two-point correlations shown in the top row of figures 10(a) & (b) for the single and co-axial cases respectively exhibit a trend very similar to those for the longitudinal velocities. For the single jet, the large scale structures identified previously along the jet centerline are responsible for the potential core instability. This is confirmed in figure 10(a) where negative peaks of radial velocity correlation are still evident for the correlation along the nozzle lipline (y/Ds=0.5). In the shear layer region, the co-axial jet exhibits continued symmetry of the correlation functions indicating uniform growth of the streamwise component extent of the turbulence scales when developing downstream as seen in the centre and lower of figures 10(b). In contrast, the single jet shows a more complex correlation pattern. The large scale structures identified previously along the jet centerline are responsible for an instability in the potential core and may be related to the helical Fourier mode described by Tinney et al (2005). This is also confirmed in figure 10(a) where negative peaks of radial velocity correlation are still manifest when the correlation is examined along the nozzle lipline (y/Ds=0.5).

The spatial correlation functions for the shear stresses u_1u_2 are reported in figure 11. Along the jet centreline, it can be seen from the top row of figure 11 that both flows exhibit anti-symmetric correlations relative to the centreline and similar to that observed by Ukeily et al (2004) in a transonic jet. For the single jet, negative and positive regions observed upstream and downstream of the reference point are indicative of flow being entrained and ejected prior to and after the reference point with a correlation of zero at the reference point. This is again indicative of the large scale coherent motion of the flow in this region of the single jet already noted. For the co-axial jet, r_{12} is somewhat different with the peak of correlation centered at the point reference and surrounded by two negative loops distant about half a diameter and exhibiting much less coherent behaviour. The differences observed along the centerline for the single and co-axial jets confirm that the reference point was located upstream and downstream the end of the potential core respectively. As the reference point is moved away from the jet centerline, significant changes are observed in the correlations shown in the centre and

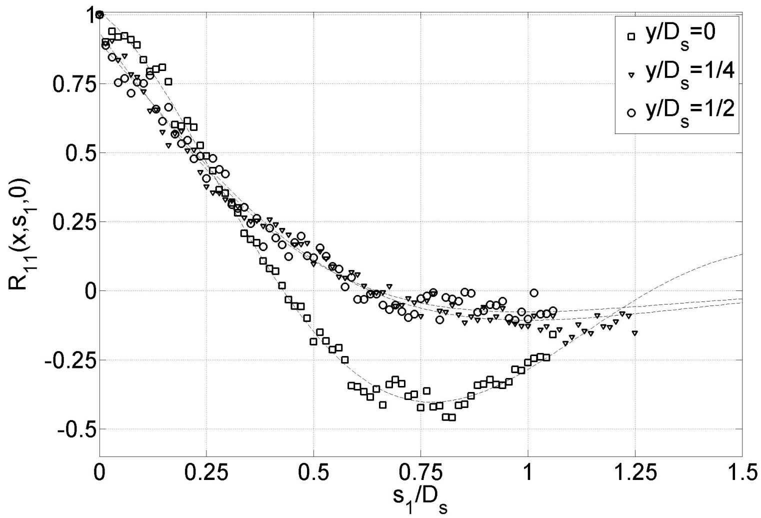

(a) $r_{11}(x, s_1, 0)$

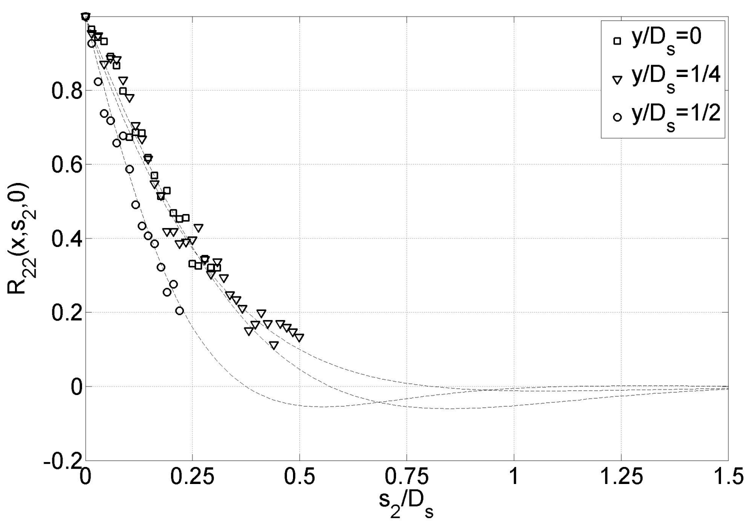

(b) $r_{22}(x, s_2, 0)$

Figure 12: Spatial correlations in *(a)* axial and *(b)* radial directions for the single stream jet. (Symbols) experiments, (dashed lines) fitting curve. Results are given with the spatial resolution of the PIV measurements.

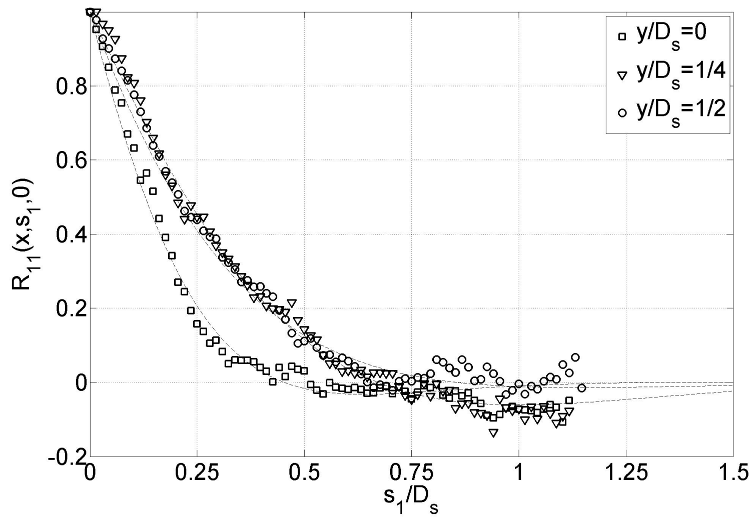

(a) $r_{11}(x,s_1,0)$

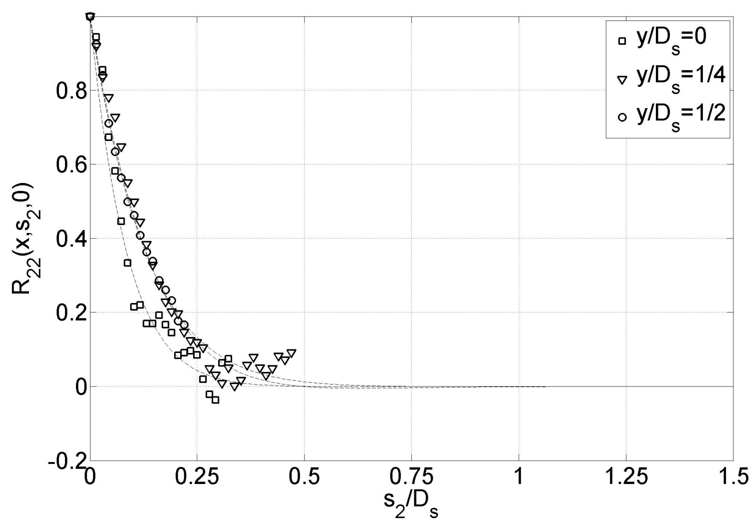

(b) $r_{22}(x,s_2,0)$

Figure 13: Spatial correlations in *(a)* axial and *(b)* radial directions for the coaxial jet. (Symbols) experiments, (dashed lines) fitting curve. Results are given with the spatial resolution of the PIV measurements.

	ii=11			ii=22		
	y/Ds=0	**y/Ds=0.25**	**y/Ds=0.50**	**y/Ds=0**	**y/Ds=0.25**	**y/Ds=0.50**
Single jet	0.89	0.52	0.45	0.3	0.29	0.21
Coaxial jet	0.16	0.26	0.25	0.09	0.12	0.13
Bridges & Wernet (2002)	0.12	0.2	0.2	0.12	0.1	0.1
Fleury et al (2007)	-	-	0.22	-	-	0.17

Table 2: Integral length scales (normalised by diameter *Ds* (=50mm)) for longitudinal and radial velocities.

lower rows of figure 11. The characteristics for both jets can be seen to be similar to those for the radial component r_{22} but extended somewhat in the streamwise direction especially for the co-axial jet. For the single stream jet, the correlation is now maximum at the reference point and the effect of the core instability on the overall correlation can clearly be seen.

4.4. Integral length scales

The length scales are calculated from the two-point correlations by extracting the spatial correlations into the main directions. The spatial correlation functions for the longitudinal and radial velocity components in the axial and radial directions respectively are reported for the three locations in both jet configurations in figure 12 and 13. Exponential cosine formulations were used to fit the experimental data and, as shown in figure 12, these provide a good fit for the data. The results for both velocity components along the centreline for the single jet case exhibit an oscillatory characteristic indicative of a dominant instability in this flow region as was seen in the auto-spectrum of figure 8(a). A more rapid decrease of the spatial correlations due to enhanced mixing is evident for the coplanar jet compared with

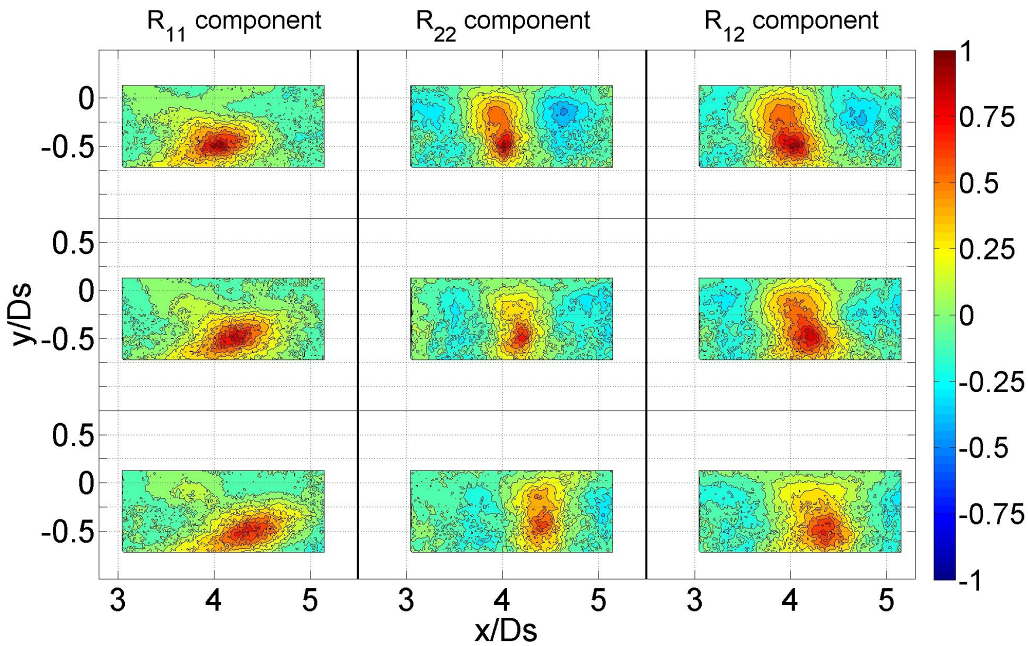

Figure 14: Two-point correlations for the single jet at various time delays $\tau Uj/D$: (top) 0, (middle) 280 and (bottom) 560.

the single jet. The integral length scales in respect of each reference point were obtained by integration of the fitting curves and the results are given in Table 2 together with the results of Bridges & Wernet (2002) for a co-axial jet. Reasonable agreement is observed for λ_{11} with an increase in the integral scale of the former towards the shear layers of the flow in both cases. For λ_{22}, an increase in the value towards the shear layers here compares with a decrease in the Bridges & Wernet data. As a short cowl nozzle was used for the latter, the integral scales in the radial would be expected to be somewhat different. Included in Table 2 are values estimated using the formulation of Fleury et al (2007) for a co-axial configuration and these show good agreement with the present results .

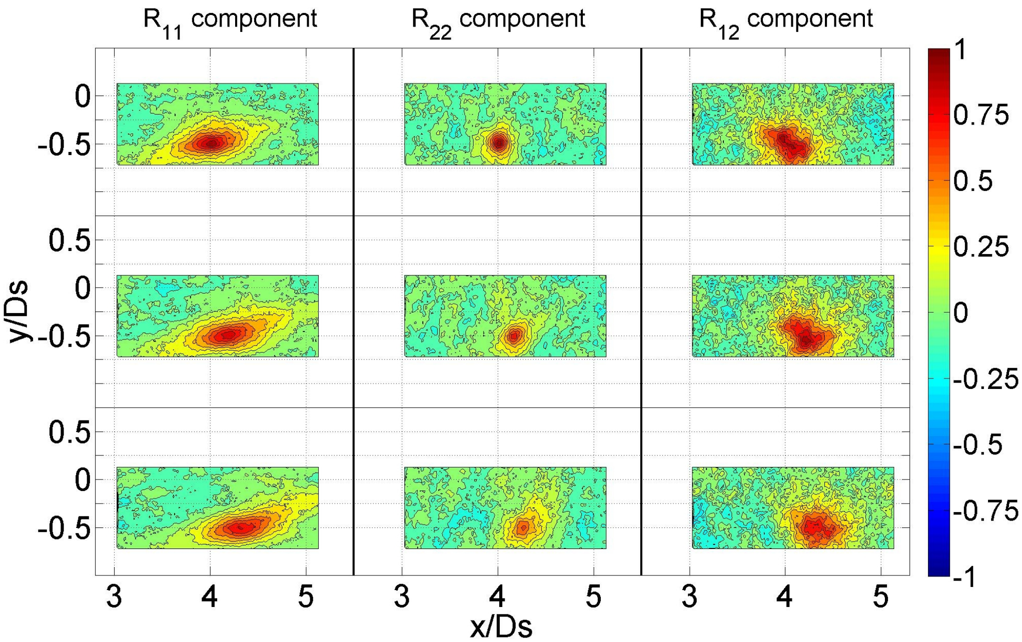

Figure 15: Two-point correlations for the coaxial jet at various time delays $\tau Us/Ds$: (top) 0, (middle) 190 and (bottom) 390.

The evolution of the integral length scale across a free shear jet flow is typically very slow as reported by, for example, Davies et al. (1963), Bridges & Wernet (2002) and Kerhervé et al. (2004) and this can be seen from figure 12 where the spatial decay at $y/D_s = 0.25$ & 0.5 are very similar. This implies that only the axial dependence of the integral scales along the jet shear layer has been required for modelling noise sources as reported by Morris & Boluriaan (2004) and Azarpeyvand et al (2006).

4.5. Temporal dynamics of the two-point correlations

Two-point spatial correlations only offer a limited view of the intrinsic dynamics of the turbulence field. The temporal decay of these correlations controls the

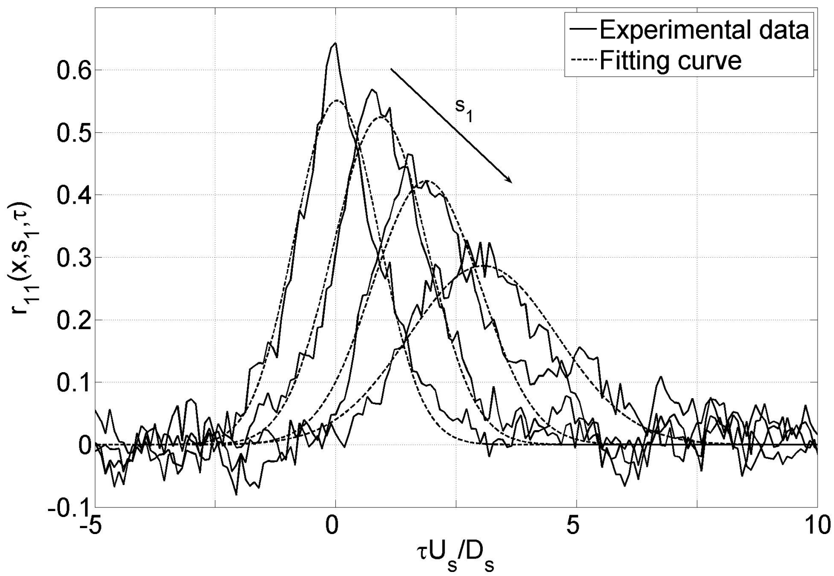

Figure 16: Temporal correlation functions $r_{11}(y,s_1,\tau)$. (solid line) Experimental data, (dashed line) Gaussian fit.

spectral dynamics of the turbulence and, as a consequence, the noise production mechanisms (Jordan & Gervais 2005). The two-point correlations r_{11}, r_{22} & r_{12} at y/Ds=0.5 are plotted in figures 14 and 15 for the single and co-axial jets respectively as a function of time. It can clearly be seen for both jets that the correlation maximum moves downstream from the reference point and decreases gradually. This is representative of turbulence convecting downstream and dissipating as a consequence of the inherent mixing processes. For both jets, the skewness of the longitudinal correlation component r_{11} is well conserved over time and the angle remains approximately constant. This would seem to confirm that this skewness is related to straining of the turbulence as suggested by Arakeri et al (2003). For the single jet flow case in figure 14, conservation of the secondary negative peaks

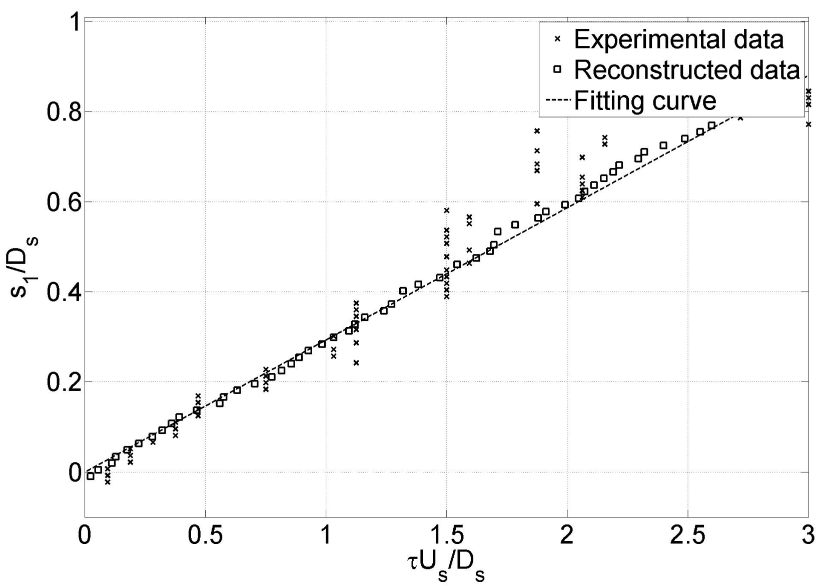

Figure 17: Distribution of time delay of the correlation peaks -$r_{11}(y,s_1,\tau)$ component shown in figure (16)- with the separation distance.

	ii=11			ii=22		
	y/Ds=0	**y/Ds=0.25**	**y/Ds=0.50**	**y/Ds=0**	**y/Ds=0.25**	**y/Ds=0.50**
Single jet	0.85	0.74	0.62	0.82	0.75	0.68
Davies et al (1963)	-	-	0.6	-	-	-
Doty & McLaughlin (2005)	-	-	0.62	-	-	-
Coaxial jet	0.80	0.46	0.29	0.80	0.50	0.28

Table 3: Convection velocities normalised by jet relative exit velocity Up.

in the radial correlation component r_{22} with increasing time delay towards the jet centerline is evident. This indicates the coherent nature of the large-scale motion identified previously as a jet instability mode.

4.6. Integral time scale and convection velocity

The moving-axis integral time scale is obtained from the two-point correlations based on a time delay as defined in equation 5 and the bulk convection velocity is given by the peak value at each separation as defined in equation 6. The convection velocity is representative of the speed at which the most coherent scales move downstream as discussed by Hileman & Samimy (2000). Typical two-point correlations obtained are reported in figure 16 for r_{11} and an iterative process based on the Nelder-Mead method (Lagarias et al 1998) [2] with Gaussian formulation was used to fit the experimental data so that the position of the peak values can be estimated. A plot of the separation distance in the axial direction as a function of the time delay is shown in figure 17 for both the raw and reconstructed data. The convection speed is determined from the average slope of the time delay with separation. It should be noted that as the degree of correlation reduces, the effect of noise will become dominant as the separation increases. The values obtained for convection velocities at the three locations are reported in table 3 for both flow configurations. For the single stream jet, the convection velocity along the nozzle lipline of 0.62 times the jet exit velocity shows good agreement with the results of Davies et al. (1963) and Doty & McLaughlin (2005) included in table 3. For both jets, similar values for the convection velocities for both longitudinal and radial velocity components are observed, although the convection speeds are significantly lower away from the jet axis in the co-axial case. Since most of the turbulent kinetic energy is transported with the main flow, convection velocities for the velocity components would be expected to be equivalent. This

[2] similar procedure than the build-in function “fminsearch’ under Matlab software.

is an important finding as the convection velocity for radial turbulence in co-axial jets has not been previously reported.

Thus, the PRGC technique is an appropriate method for the estimation of convection velocities. It should be noted that the determination of convection velocities from either high speed PIV or single point measurements requires significantly more data than for the PRGC approach.

5. Conclusion

The Point-Referenced Global Correlation (PRGC) technique of Chatellier & Fitzpatrick (2005) combining PIV and simultaneous LDV measurements has been used to determine two-dimensional two-point space time turbulence correlations for both single and co-axial jet flows at a Mach number 0.24. The results have implications for noise prediction techniques based on the acoustic analogy as these require models for the two-point space time correlation tensor of the turbulence.

From the results presented, it has been shown that the technique can highlight specific features of the flow such as anisotropy of the turbulence, straining effects due to the presence of shear layer gradients and the convection and dissipation of the turbulence as the flow progresses downstream from the nozzle exit. For the single jet, a strong instability mode at the end of the potential core was identified and it was shown that its presence significantly affects the correlation function. For the co-axial jet, the integral scales have been shown to agree well with values from the literature and the convection speeds are reported here for both longitudinal and radial scales.

The results show clearly that the PRGC technique is an effective method for determining both the spatial and temporal dynamics of the flow compared with the use of unsteady PIV or multi two point measurements where significantly more data and processing time is required.

Part of this work was funded by the EU project COJEN (Computation of Co-Axial Jet Noise) funded under the EU FP6 programme as contract no AST3-CT-2003-502790.

References

Arakeri L, Krothapalli A, Siddavaram V, Alkislar MB, Lourenco LM (2003), On the use of microjets to suppress turbulence in a Mach 0.9 axisymetric jet. J Fluid Mech, 490: 75-98

Azarpeyvand M, Self RH, Golliard J (2006) Improved jet noise modelling using a new acoustic time scale. 12th AIAA/CEAS Aero Conf, AIAA Paper 2005-2598

Bassetti A, Morfey L (2007) An acoustic-analogy model for jet noise prediction. 13th AIAA/CEAS Aero Conf, AIAA Paper 2007-2977

Batchelor GK (1953) The theory of homogeneous turbulence. Cambridge University Press

Bogey C, Bailly C (2005) Investigation of sound sources in subsonic jets using causality methods on LES data. 11th AIAA/CEAS Aero Conf, AIAA Paper 2005-2886

Bridges J, Wernet MP (2002) Turbulence measurements of separate flow nozzles with mixing enhancement features. 8th AIAA/CEAS Aero Conf, AIAA Paper 2002-2484

Chatellier L, Fitzpatrick J (2005), Spatio-temporal correlation analysis of turbulent flows using global and single-point measurements. Exp In Fluids, 38(5): 563-757

Chu WT (1966) Turbulence measurements relevant to jet noise. Univ Toronto Inst Aero Studies UTIAS Report 119

Davies POAL, Fisher KJ, Barrat MJ (1963) The characteristics of turbulence in the mixing region of a round jet. J Fluid Mech, 15: 337-367

Delville J, Ukeily L, Cordier L, Bonnet JP, Glauser M (1999) Examination of large-scale structures in a turbulent plane mixing layer. Part 1: Proper Orthogonal Decomposition. J Fluid Mech, 391: 91-122

Doty MJ, McLaughlin DK (2005) Space-time correlation measurements of high-speed jets using optical deflectometry. Exp in Fluids 38(4):415-425

Fisher MJ, Davies POAL (1964) Correlation measurements in a non-frozen pattern of turbulence. J Fluid Mech, 18: 313-356

Fleury V, Bailly C, Michard M, Juv D, Jondeau E 2007, Measurement by Dual-PIV of space-time correlation scales in subsonic jets. 13th AIAA/CEAS Aero Conf, AIAA Paper 2007-3615

Goldstein ME (1976) Aeroacoustics. McGraw-Hill

Hileman J, Samimy M (2000) An attempt to identify noise generating turbulence structures in a high speed axisymetric jet. 9th AIAA/CEAS Aero Conf, AIAA Paper 2000-2020

Hileman J, Thurow B, Caraballo E, Samimy M (2005) Large-scale structure evolution and sound emission in high-speed jets: real-time visualisation with simultaneous acoustic measurements. J Fluid Mech, 544

Hu H, Saga T, Kobayashi T, Taniguchi N (2002) Simultaneous measurements of all three components of velocity and vorticity vectors in a lobed jet flow by means of dual-plane stereoscopic particle image velocimetry. Phys Fluids, 14(7): 2128-2138

Hussain AKMF, Clark AR (1981) On the coherent structure of the axisymmetric mixing layer: a flow visualization study. J Fluid Mech, 104:263-294

Jordan P, Gervais Y (2005) Modelling self and shear noise mechanisms in inhomogeneous, anisotropic turbulence. J Sound Vib, 279: 529-555

Jung D, Gamard S, George WK (2004) Downstream volution of the most energetic modes in a turbulent axisymmetric jet at high Reynolds number: part 1. The near-field region. J Fluid Mech, 514: 173-204.

Kerhervé F, Jordan P, Gervais Y, Valière JC, Braud P (2004) Two-point Laser Doppler velocimetry measurements in a Mach 1.2 cold supersonic jet for statistical aeroacoustic source model. Exp in Fluids, 37(3): 419-437

Kerhervé F, Fitzpatrick J, Chatellier L (2008) A sensitivity analysis of the point reference global correlation (PRGC) technique for spatio-temporal correlations in turbulent flows. Exp in Fluids, 44(4): 577-589.

Ko NWM, Kwan AS (1976) The initial region of a subsonic jet. J Fluid Mech, 73(2):305-332

Lau JC, Morris MJ, Fisher MJ (1979) Measurements in subsonic and supersonic free jets using laser velocimeter. J Fluid Mech, 93(1): 1-27

Lagarias JC, Reeds JA, Wright MH, Wright PE (1998) Convergence properties of the Nelder-Mead Simplex method in low dimensions. SIAM J of Optimization, 9(1): 112-147 **Lau JC** (1980) Laser Velocimetry correlation measurements in subsonic and supersonic jets. J Sound Vib, 70(1): 85-101

Laurendeau E (2007) Etude aéroacoustique d'une méthode de contrôle d'un jet subsonique par fluidevrons, PhD Thesis, Université de Poitiers, France

Liepman HW, Laufer J (1947) Investigations of three turbulent mixing.

NACA Technical Note, no 1257

Lighthill MJ (1952) On sound generated aerodynamically. Part I: General theory. Proc Roy Soc, A(211): 564-587

Morris JM, Boluriaan S (2004) The prediction of jet noise from CFD Data. 10th AIAA/CEAS Aero Conf, AIAA Paper 2004-2977

Muller E, Nobach H, Tropea C (1998) A refined reconstruction-based correlation estimator for two-channel, non-coincidence Laser Doppler anemometry. Meas Sc Technol, 9: 442-451

Nobach H, Muller E, Tropea C (1998) Efficient estimation of power spectral density from laser Doppler anemometer data. Exp in Fluids, 24(5/6): 499-509

Ricaud F (2003) Etude de l'identification des sources acoustiques à partir du couplage de la pression en champ proche et de l'organisation instantannée de la zone de mélange de jet, PhD Thesis, Université de Poitiers, France

Ribner HS (1969) Quadrupole correlations governing the pattern of jet noise. J Fluid Mech, 38: 1-64

Self RH (2004) Jet noise prediction using the Lighthill acoustic analogy. J Sound Vib, 275, 757-768

Tennekes H, Lumley JL (1972) A First Course in Turbulence, MIT Press

Tinney C, Glauser M, Ukeily L (2005) The evolution of the most energetic modes in a high subsonic Mach number turbulent jet. 43rd AIAA Aerospace Meeting, AIAA Papper 2005-0417

Townsend AA (1974) The Structure of Turbulent Shear Flows. Cambridge University Press.

Ukeily L, Tinney C, Mann R, Glauser M (2004) Spatial correlations in a transonic jet. 34th AIAA Fluid Dyn Conf Exh, AIAA Paper 2004-2654

Westerweel J (2000) Theoretical analysis of the measurements precision in particle image velocimetry. Exp In Fluids, 29: S3-S12.